Supporting Information

A stretchable PVA-agar hydrogel patch embedded with metal-doped carbon dots (MCD) for monitoring the Ca^{2+} biomarker

Lingaraj Behera,[a] Sasmita Mohapatra[a,b]*

[a]Department of Chemistry, National Institute of Technology, Rourkela, India-769008

[b]Centre for Nanomaterials, National Institute of Technology, Rourkela, India-769008

*Corresponding author: Tel: 91-661-2462661, Fax: 91-661-2472050,

*E-mail: sasmitam@nitrkl.ac.in

Number of pages: 21

Number of figures: 14

Number of schemes: 2

Number of tables: 4

Contents in the supporting information:

Figure S9 (a) Adhesiveness of the hydrogels on human skin (b) photographs of the hydrogel attached to the arm of a human body for 8 hours, no allergic reaction was observed after picking up (c) The water absorption speed and (d) water retention rate of the hydrogel patch.

Figure S10 (a)FL detection of Ca^{2+} in aqueous solution (b) linear fitting of detection range (c) selectivity study for cation in aqueous phase (d) selectivity study for anion in aqueous phase

Figure S11 (a)FL life time study of MCD and MCD + Ca^{2+} (b) DLS size MCD and MCD +Ca^{2+} (c)Zeta potential study of MCD and MCD + Ca^{2+}

Figure S12 (a) Repeatability study of MCD@PAGH (b) Stability of MCD@PAGH (C) Ca^{2+} ion detection in sweat release from hand, shoulder, knee

Figure S13 (a)Mobile set up for RGB app-based detection(c) stability of the patch

Figure S14 PAGH after addition of Ca^{2+} ion

1.Instruments

UV-visible absorption and fluorescence spectra were examined by using a UV-VIS spectrophotometer (Shimadzu 2650) and a spectrofluorometer (Quantamaster, Horiba-PTI). Zeta potential analysis was examined by using a zeta sizer Nano ZS 90, Malvern instrument. Surface functional groups was checked by using Fourier Transform Infrared Spectroscopy (FTIR) (IRAffinity-1S, Shimadzu, spectrophotometer). The morphology and elemental distribution of the MCD was observed by using a Table Top scanning electron microscope (Hitachi, FlexSEM1000 II). Transmission electron microscope (FEI, Tecnai G2 TF30-ST) was used to know the structure and shape of the MCD. The surface composition of MCD and hydrogel was obtained by X-ray photoelectron spectrum (XPS) recorded by (PHI 5000 VersaProbe III). Powder X-ray diffractometer (XRD) (RIGAKU, JAPAN & ULTIMA-IV) was used to obtained the crystallinity and phase analyzer of the synthesized material. A Bruker Multimode-8 atomic force microscope (AFM) was used to examined the surface topography and sample roughness. The average fluorescence lifetime was calculated by using a Horiba Jobin von TCSPC (time-correlated single-photon counting technique). Using FL spectrophotometer with an integrating sphere and the software Felix GX 4.1.2, the absolute fluorescent quantum yield is calculated.

2. Experimental section

2.1 Fabrication of MCD

Citric acid, EDTA-2Na.$2H_2O$, and $CuCl_2.2H_2O$ were used as sources to make MCDs through a simple hydrothermal method. The hydrothermal carbonization of the EDTA-Cu chelate is the mechanism for the production of MCD. 4 g citric acid, 2.5 g EDTA-2Na.$2H_2O$ and 20mg $CuCl_2.2H_2O$ were typically dissolved in 20 mL deionized water while stirring, followed by filtering to remove undissolved EDTA.The solution was then poured into a teflon-lined autoclave and heated continuously at 200^0C for 8 hours. The products with large size particles were directly remove from the resulting solution by centrifugation at 8000 rpm for 15 min after the reaction cooled to room temperature. The as-synthesized products containing the solution were further purified in a dialysis bag (retained molecular weight: 500 Da) against millipore water for 24h to obtain MCDs. The purified MCD solution was then freeze-dried in a vacuum to produce MCD nanoparticles. The MCD particles were then redispersed in ultrapure water and stored at 4^oC for further characterization and application. On the other hand, the same process was used to make CDs without metal doping (EDTA-2Na.$2H_2O$, citric acid as a precursor). Various reaction conditions like reaction temperatures and time were optimized

to reach the best fluorescence property of synthesized MCD. After optimization, temperature and time have been fixed at 200°C for 8h to get MCD with best fluorescence property.[1]

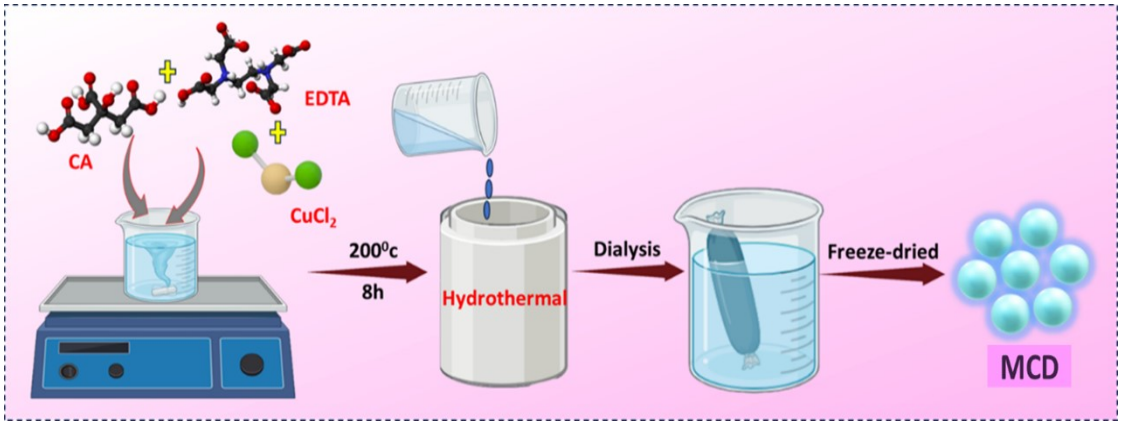

Scheme S1 Synthesis of MCD

2.2 Preparation of a wearable MCD@PAGH fluorescence patch

A hydrogel with a diameter of 5 mm and a thickness of 3 mm was removed from the template of microporous hydrogel were manually produced on it with a puncher.

2.3 Preparation of artificial sweat

Artificial sweat was prepared by a mixed solution containing 17.5 gL^{-1} NH_4Cl, 20 g L^{-1} NaCl, 2.5 g $L^{-1}CH_3COOH$,5g L^{-1}urea and 15g L^{-1} lactic acid and its pH was adjusted to 4.5–5.5 using NaOH.[2]

2.4 Characterization study of MCD@PAGH

2.4.1 Microscopic charcterization of the hydrogel

The microstructure of the PAGH and MCD@PAGH was observed by a scanning electron microscope (JEOL JSM-6480LV) at 15 kV. Hydrogels with a diameter of 24 mm and height of 11 mm were frozen with liquid nitrogen and then vacuum freeze-dried for 48 h. The dried hydrogels were cut along the cross section and placed on the SEM platform to be sputtered with gold. The microstructure was observed at 50 and 500× magnifications. At least 20 data points were collected to calculate and analyze the pore size of the hydrogels using the imagej.

2.4.2 Rheological properties of MCD@PAGH

The Rheolab QC Anton Paar was used for rheological measurements of hydrogels. MCD@PAGH were made into cylinders with a thickness of 5 mm and a diameter of 10 mm, and each hydrogel contained a different amount of MCD. At the time of experiment, the sample temperature was kept at a constant 30°C.

2.4.3 Swelling ratio study of MCD@PAGH

The hydrophilicity of MCD@PAGH was obtained by following an equilibrium swelling method. The hydrogels were freeze-dried overnight for complete removal of water. Then the dry-hydrogel were weighed and placed in a beaker containing 30 mL of double distilled water. In regular interval of time, the wet hydrogel was taken out from the beaker and the excess surface water was removed by using tissue paper. Then, the weight of the wet hydrogel was noted down and again dipped in beaker for further study. The swelling ratio of the hydrogels were calculated by using the following equation.

$$\text{Swelling ratio (\%)} = \frac{Wt - Wo}{Wo} \times 100 \quad \text{----------(1)}$$

where w_t is the weight of the hydrogel after swelling at different times, and w_0 is the initial weight of the hydrogel. Data from each hydrogel specimen was calculated three times.

2.4.4 Mechanical property test of MCD@PAGH

A universal tensile machine (INSTRON Electroplus E1000 and E3000 test system) was used to calculate the mechanical properties of the hydrogel samples. According to the tensile test requirements, the hydrogel was prepared into square shape (length, width, and thickness were 35, 10, and 5 mm respectively), and the tensile speed was fixed at 40 mm/min. According to the compression test requirements, the hydrogel was prepared cylindrical shape (diameter and height were 15 mm and 20 mm). The compression speed was set at 5 mm/min.

The tensile strain (ε_T%) is calculated as follows:

$$\varepsilon_T = \frac{l}{lo} \times 100 \quad \text{---------- (2)}$$

where the l and l_0 respectively represent the immediate length and original length of the test spline, and the unit is mm.

The compression strain (γ_c%) is calculated as follows:

$$\gamma_c = \frac{h}{h0} \times 100 \quad \text{---------- (3)}$$

where the h and h_0 respectively represent the immediate height and original height of the test spline, and the unit is mm.

The stress (σ, kPa) is calculated as follows:

$$\sigma = \frac{F}{W \times H} \quad \text{---------- (4)}$$

where F stands for load and the unit is N; W represents the width of the test spline, and H represents the spline thickness. The unit of W and H is mm.

The fracture energy of the MCD@PAGH was determined according to the literature.[3] Specifically, the MCD@PAGH was prepared as a rectangular sample and there was an initial notch at the midpoint of the short edge of the hydrogel sample. The formula of fracture energy

$$G = \frac{2F}{h} \quad \text{---------- (5)}$$

where F is the loading force and h is the thickness of the MCD@PAGH

2.4.5 Self-Healing performance test of the MCD@PAGH

The self-healing properties of hydrogels were mainly studied by the direct observation method and instrument testing method. A whole hydrogel was cut into two parts. One of them was stained with malachite green, while the other was not stained. Then, the fracture surface of the two parts was spliced together at room temperature. First of all, after 24h of self-healing, the self-healing effect was observed by manually stretching.

2.4.6 Adhesion performance test of the MCD@PAGH

Initially, visual experiments were conducted to determine the adhesion properties of MCD@PAGH on various substrates. Subsequently, the adhesive nature of the hydrogel was assessed in a quantitative manner through the utilisation of a universal testing machine. The specific process was to bond the hydrogel to the substrate for 2 minutes and then stretch it at 40 mm/min until the substrate and hydrogel were totally separated. Combined with the maximum tensile strength, the adhesion strength (FA) of the hydrogel to the materials can be calculated. The calculation method is as shown in the formula:

$$F_A = \frac{F}{S} \times 100 \quad \text{---------- (6)}$$

where F is the maximum tensile force during the stretching process and S is the contact area of the hydrogel with the tested material.

2.4.7 Procedure for detection of Ca^{2+}

To analyse the fluorescence response of the MCD towards Ca^{2+}, a solution containing 1µM $CaCl_2$ was prepared. Various concentration of Ca^{2+} solution was made by diluting the stock solution using PBS buffer (pH 8, 0.1M). Subsequently, 20µL of the MCD was added with different concentration Ca^{2+} (3mL total volume). The resulting mixtures were vigorously agitated and shaken for a duration of 15 minutes at 25°C. After 15 min of incubation, the fluorescence intensities were measured using a spectrofluorometer (Horiba-PTI, QM-400) at an excitation of 380 nm. To construct the calibration curve, the concentration of Ca^{2+} was plotted on the X axis, while relative intensity (F_0/F) was plotted on the Y axis. Here, F_0 and F represent the intensities of Ca^{2+} at concentrations 0 and C, respectively. To verify the selectivity of the MCD probe towards Ca^{2+}, the FL responses of the MCD towards other anions and cations were compared.

2.4.8 Detection of Ca^{2+}through electrochemical measurement

First, a small piece of MCD@PAGH with a height of 15 mm and width of 10 mm was cut from a MCD@PAGH with a diameter of 55 mm and mounted between two custom made Teflon modules. Transmembrane ionic currents were measured using a Keithley 6487 picoammeter. A pair of Au probe were applied a voltage sweep from −5 to +5 V with a step voltage of 0.25 V. The ionic current of the PAGH was assigned as the initial current value. Then, a series of different concentrations of analyte (including various calcium ions and other anions and cations) solutions were added based PAGH. Before each test, analyte solutions were drop wise added to PAGH patch and the corresponding ionic currents were recorded after the 10 min of analyte absorption. The practical application of MCD@PAGH patch in electrochemical sensing of Ca^{2+} in real sweat samples was explored on volunteers during commencement of certain physical activities.

2.4.9 On-body testing of the wearable hydrogel patch (Band-aid)

We made a band-aid set up for the on-body sweat analysis. After removing the cotton from the band-aid, hydrogel patch is attached directly to band-aid. A group of 3 healthy young adults participated in the test as volunteers and gave informed consent. An in situ Ca^{2+} test in sweat was performed on three healthy volunteers, whose skin was cleaned with a medical cotton swab and then worn with a MCD@PAGH patch attached band-aid. Then, volunteers ran on a treadmill at a steady pace until they broke into a sweat, after that band-aid was removed. SAMSUNG M51 mobile phone was used to take a picture of the wearable hydrogel patch under UV lighting and the RGB composition of the target position was analyzed through the color recognizer application to read the target concentration.

2.4.10 Smartphone app for fluorometric hydrogel patch sensing platform

Fluorescent hydrogel patch was made to get visual detection of Ca^{2+} in sweat. Moreover, the analyses are often limited to semiquantitative monitoring and cannot acquire high accuracy because it is tough

to distinguish a slight color variation that just relies on our naked eyes. For minimizing environmental factor (relative position between sample and camera and light source intensity) and operation error (information extraction and transformation), a handmade device was proposed to solve the current limitations of image-capturing instability and image-processing complexity. In this study, a portable platform consisting of a smartphone, a dark box connecting with the smartphone, an optical filter holder to load the filter, a UV lamp holder to fix a mini-UV lamp, and a sample slot to place the hydrogel patch was constructed. The corresponding models and the design parameters of these accessories, hardware set up, are presented in our previous work.[4] When adding a different concentration of Ca^{2+} ion and as well as sweat, the prepared hydrogel patch displayed color changes from cyan blue to dark blue. Then the smartphone captured the corresponding fluorescence photos and output the RGB values through a colour recognition RGB APP installed on the smartphone to perform quantitative detection.

3. Result and Discussion

3.1 Morphology analysis of MCD

The size and morphology of the MCDs were examined using TEM and the image is shown in (Fig. S1a). The MCDs were uniformly dispersed and spherical with well-resolved lattice fringes in HRTEM image displaying the interplanar spacing at 0.24 nm, which corresponds to the (002) facet of CDs (inset in fig S1a). The particle size distribution curve for the MCDs, with an average size of 6 nm is presented in (Fig. S1b). The "Tyndall effect" of the MCD aqueous dispersion further confirmed the quantum dot behaviour (the inset of fig. S1b). To further analyze the roughness of the MCD, the atomic force microscopy (AFM) analysis was carried out (Fig. S1c). The topographic heights (Fig. S1d) calculated from the AFM analysis suggest that MCD possesses thickness of about 10 nm which compliments TEM result. The phase purity and structural stability of the resulting MCD and MCD@PAGH was characterized by XRD. As shown in figure 1e, the X-ray diffraction (XRD) pattern of the PVA solid shows three typical peaks at 2θ = 40.8°, 22.9°,19.6° assigned to the (102), (200), (101) planes of PVA crystallite.[5] It could be seen that carbon dot shows a broad diffraction peak at 24.42° corresponding to (002) planes which was assigned to the amorphous nature of MCD. The PAGH show similar XRD patterns as PVA, suggesting the presence of PVA crystallites. MCD@PAGH prepared with a different MCD concentration of 0.5, 2.0, and 4.0 mg/ml reveal that addition of amorphous MCD leads to the decreased crystallinities of the hydrogels because the fast formation of H-bond in PVA-agar aggregates at a high temperature.

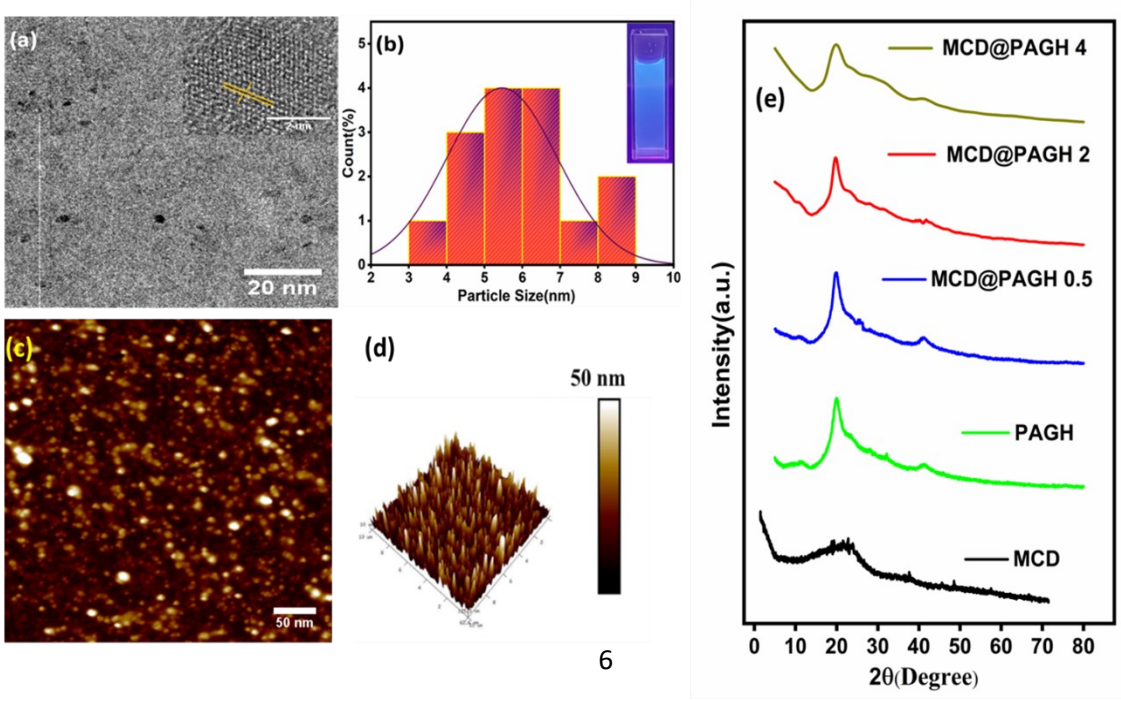

Figure S1(a) TEM image of MCD (b) particle size distribution of MCD (c) AFM image of MCD (d) Topographic height of MCD (e) XRD of the PAGH with MCD@PAGH

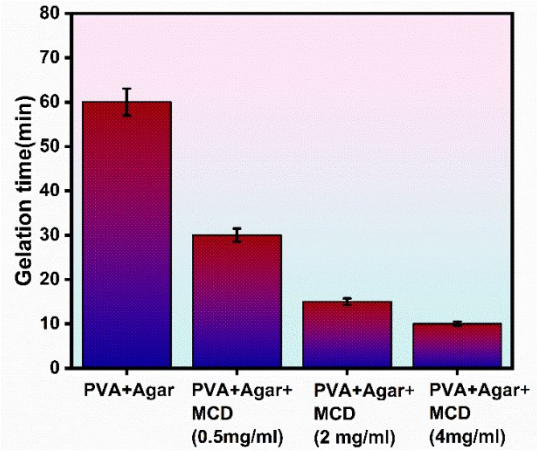

Figure S2 Gelation time of MCD@PAGH with variable amount of MCD

3.2 Microstructure of PAGH and pore size of MCD@PAGH

The microstructures of the PAGH are shown in S3. It can be clearly seen that all hydrogels showed interconnected porous structures with pore sizes on the micrometer scale. Fig. S3 a-a', b-b', c-c, d-g shows the microporous structure of the PAGH. The pore size structure of the PAGH was clear and regular, with an average pore size of 25-35 µm. The porous structure provides a high specific surface area and sufficient space, which facilitates the capture of more active materials. After incorporating MCD into the PAGH, the structure of hydrogels became increasingly regular, with significantly smaller pores and smoother connections. The pore sizes of PAGH, MCD@PAGH 0.5, MCD@PAGH 2, MCD@PAGH 4 were 25–35 µm, 18–28 µm, 15-22 µm, and 15–18 µm respectively. This indicated that the introduced MCDs can be evenly distributed in the hydrogels and make the network structure of the hydrogels denser by cross-linking with the hydrogels.

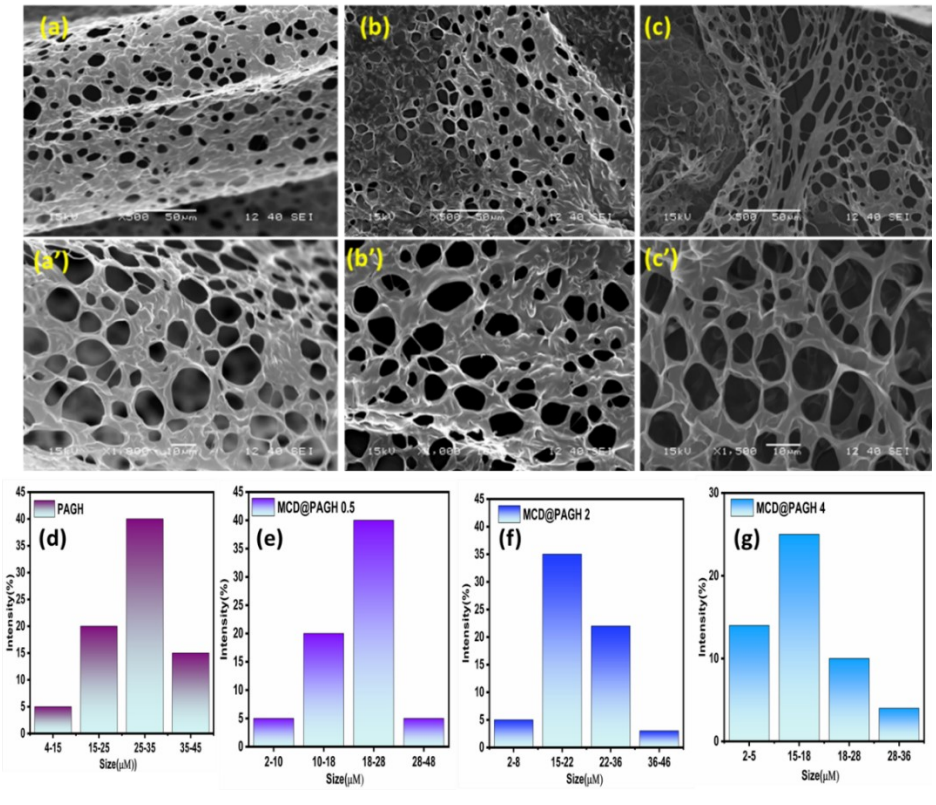

Figure S3 SEM image of PAGH (a-a', b-b', c-c') and pore size distribution of hydrogels (d) PAGH, (e) MCD@PAGH 0.5, (f) MCD@PAGH 2 (g) MCD@PAGH 4

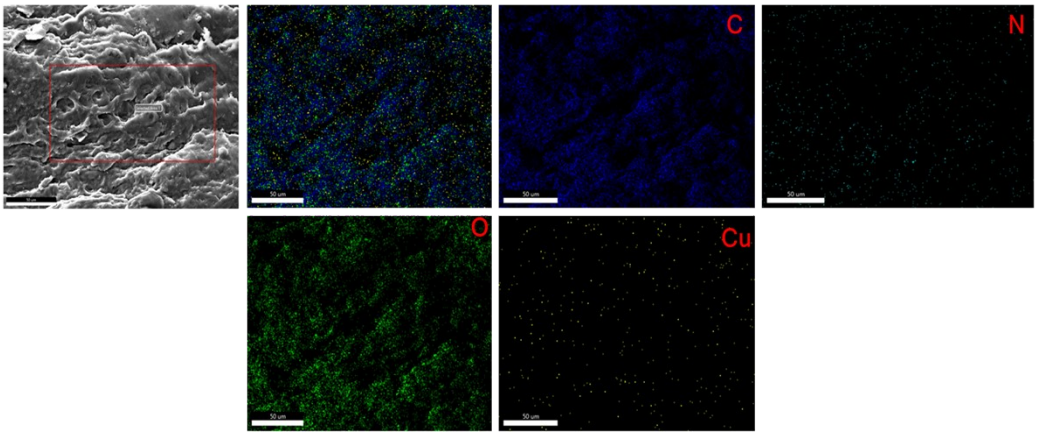

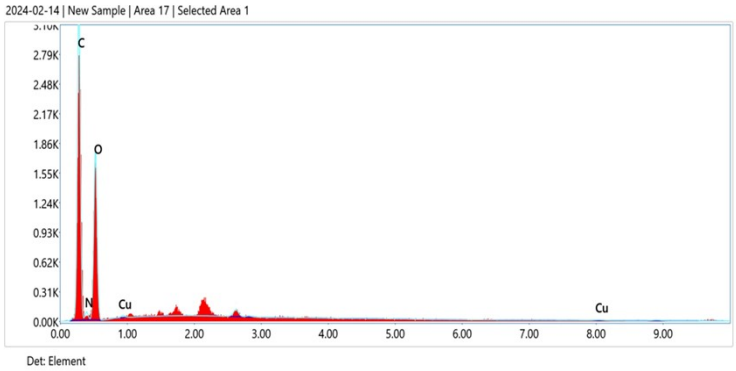

Element	Weight %	Atomic %	Net Int.	Error %
C K	63.9	70.4	585.4	8.5
N K	3.9	3.6	15.4	18.9
O K	31.7	25.8	349.6	10.6
Cu K	0.5	0.2	23.1	18.4

Figure S4 EDX and elemental mapping of MCD@PAGH

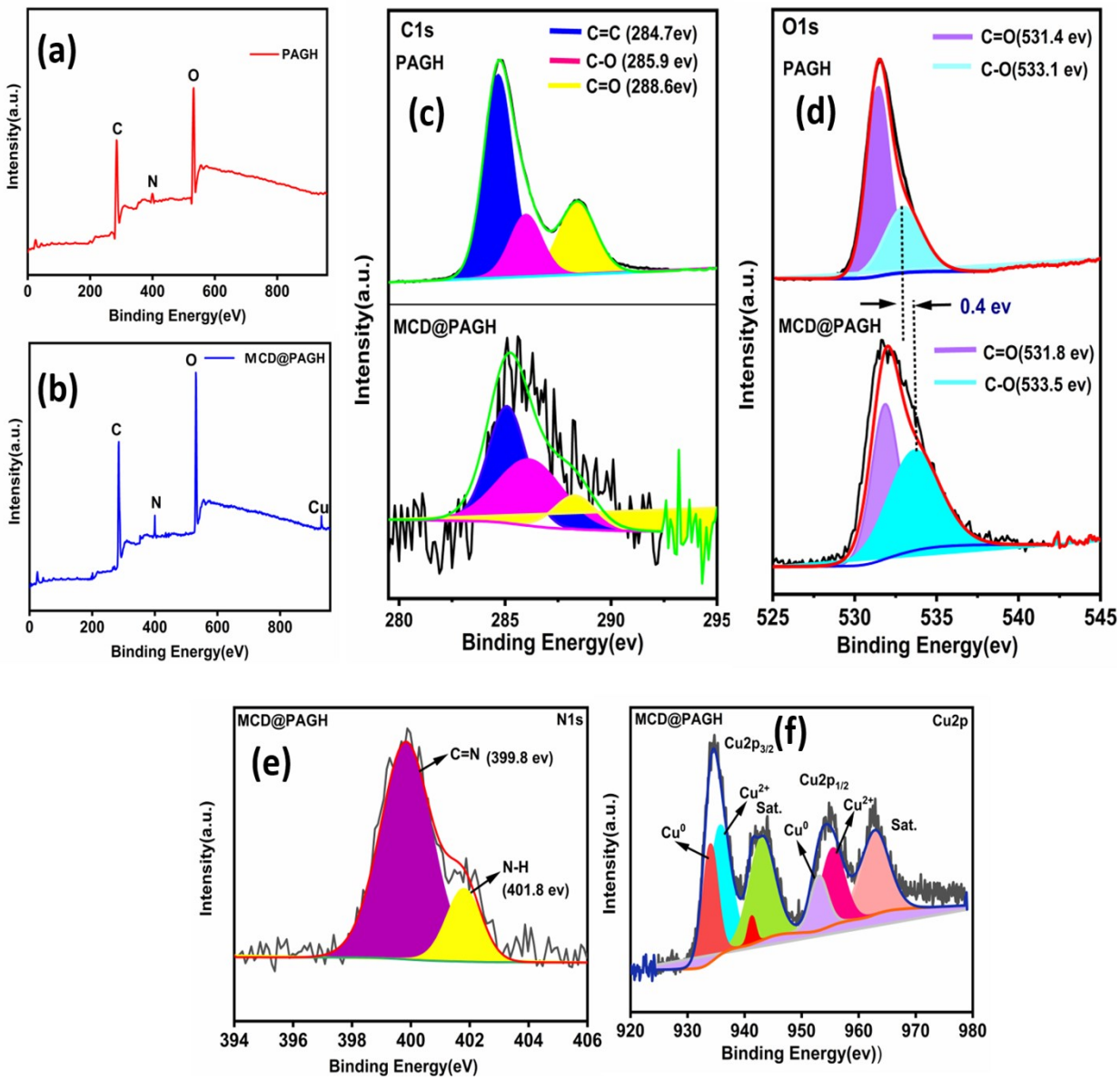

Figure S5 XPS peak of PAGH and MCD@PAGH

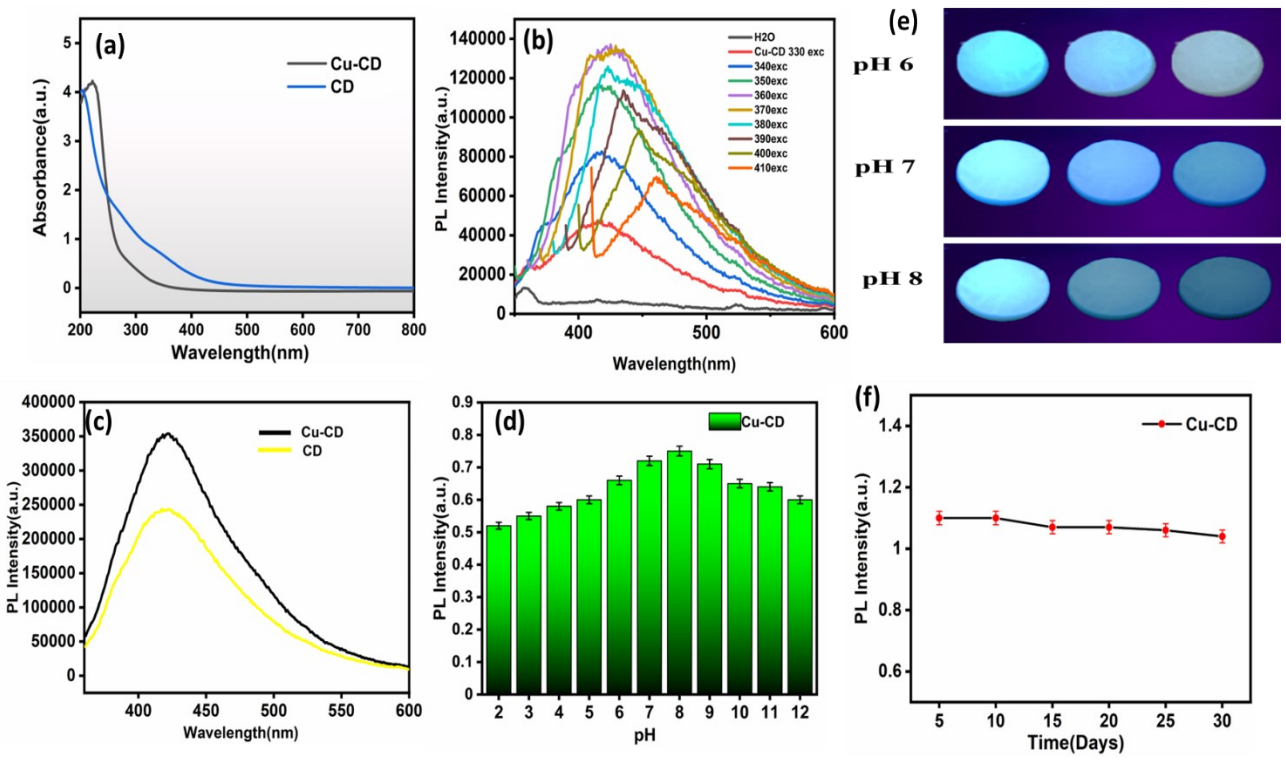

Figure S6 (a) UV-visible absorption spectra (b) excitation dependent emission spectra of MCD(c) Comparison of CD and MCD (d) pH of MCD(e) FL intensity of patch at pH (6-8) after Ca^{2+} addition (f) stability of MCD

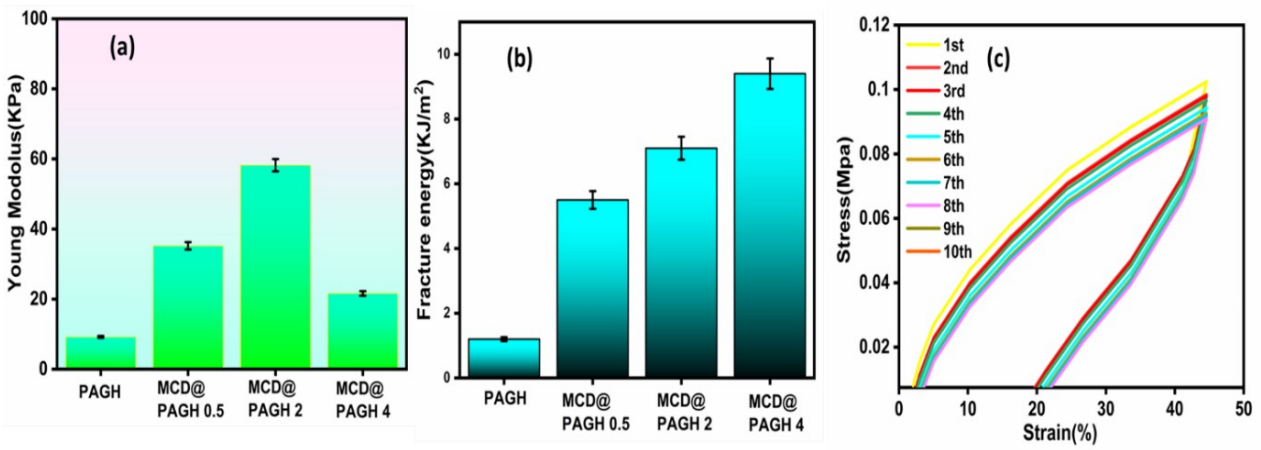

Figure S7(a)Young modulus of MCD@PAGH(b)fracture energy of MCD@PAGH(c) tensile cycle study of MCD@PAGH

3.3 Rheological properties and swelling behaviour of MCD@PAGH

The rheological study was examined to know the viscoelastic properties of the MCD@PAGH, which was checked at a varying angular frequency of 1-10 rad/s. As shown in figure S8a, the storage modulus (G′) of each synthesized specimen are higher than the loss modulus (G″), which indicated the formation of gel and all gels are showing solid like elastic nature rather than viscous nature. As expected, the G′ and G″ of all the hydrogels were relatively stable, due to the large surface functionalization units of MCD. We also found that G′ and G″ values of the hydrogel increased with the increase of MCD content, this was because MCD could form a large number of hydrogen bonds with agar and PVA, which increased the strength of the gels. Swelling resistance is a vital issue for hydrogel sensors. The swelling behaviour of the MCD@PAG**H** in water mainly depends on the competition between the hydrophobic interactions and electrostatic interaction in the gel network. Figure S8b showed that, in PAGH with different MCD amount had a large swelling ratio and swelling percentage continued to increase over 48h period. A comparison in figure 8c shows that the swelling rate was PAGH > MCD@PAGH 0.5 > MCD@PAGH 2 > MCD@PAGH 4. After 48h of swelling, the swelling rates of PAGH**,** MCD@PAGH 0.5**,** MCD@PAGH 2 and MCD@PAGH 4 were 990.65 %, 773.88 %, 711.92 % and 645.45 % respectively. It was confirmed that the swelling ratio of hydrogel decreased with the increase of MCD content, this is due to the increase of MCD enhances the hydrogen bonding in the hydrogel system, which forms a denser hydrogel network with reduced pore size and lower swelling ratio. The water evaporation ratio of hydrogels with different MCD contents was shown in figure S8d. The water evaporation ratios of all specimens were fast in the first 12h, and then subsequently slowed down. The PAGH with 2% and 4% MCD still retained a certain amount of water at 24 h and 48 h, like swelling ratio, the water evaporation ratio of hydrogels also decreased with increasing MCD content for the same reason mentioned above. The stronger the interaction between the components of the hydrogel and the smaller the pore size, the more difficult it is for water molecules to escape from the interior of the hydrogel.

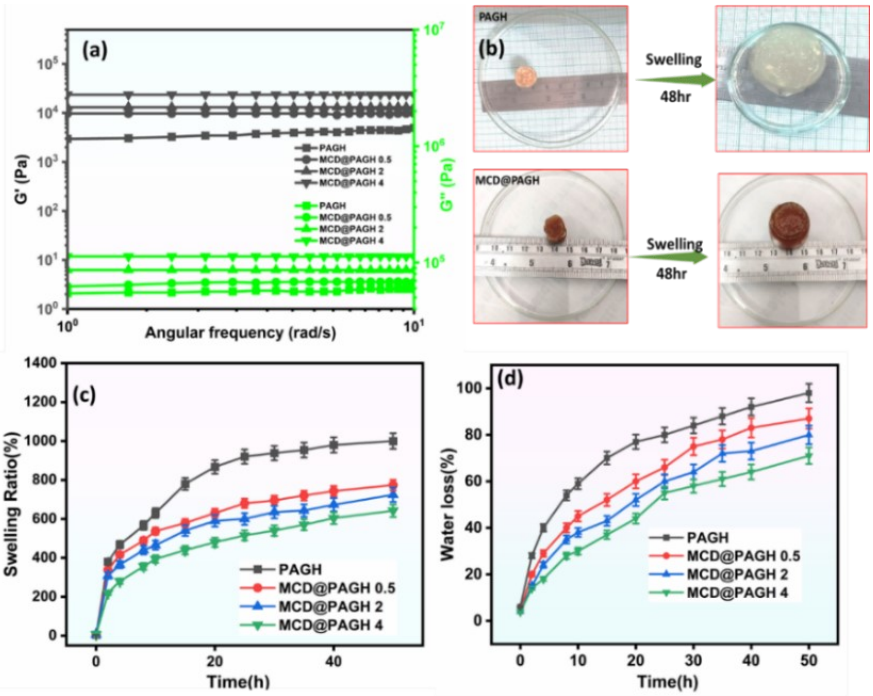

Figure S8 (a) Rheology study of MCD@PAGH with different MCD concentrations (b) swelling image of PAG and MCD@PAGH (C) Swelling ratio of hydrogel with respect to time(d) the water evaporation of hydrogels with different MCD concentrations

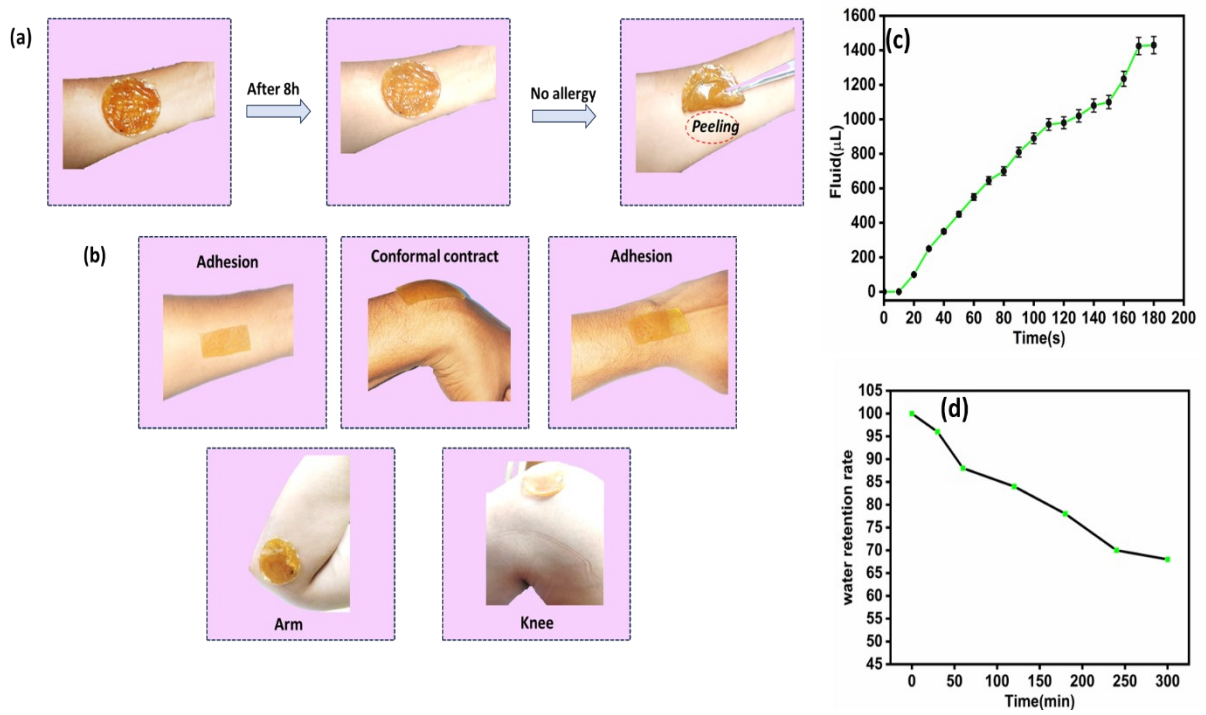

Figure S9 (a) Adhesiveness of the hydrogels on human skin and no residue was observed (b) The photographs of the hydrogel attached to the arm of a human body for 8 hours, no allergic reaction was observed after picking up, The water absorption speed (c) and the water retention rate (d) of the hydrogel patch.

3.4 Fluorescence detection of Ca^{2+} in aqueous phase

The response of MCDs toward Ca^{2+} ion was analysed from FL intensity of aqueous dispersion of MCD in variable concentrations of Ca^{2+}. It is shown that with an increase in Ca^{2+} concentration, the fluorescence intensity of aqueous solution of MCD linearly decreases at 445 nm within concentration range 5-300 µM with a correlation coefficient of 0. 997 (Fig S10a). The detection limit (LOD) of MCDs toward Ca^{2+} ion was measured to be 47.51µM using LOD formula 3 SD/ṗ, where SD refers to standard deviation and ṗ slope of linear regression curve (Fig.S10b).[6] The FL response of MCD was recorded with cations and anions under the same conditions in order to test its selectivity for calcium. Also, the fluorescence intensity of MCD toward Ca^{2+} at 445 nm was unaffected by the presence of other cation and anions (Fig S10c, d). These findings validated the high selectivity of MCD for Ca^{2+}.

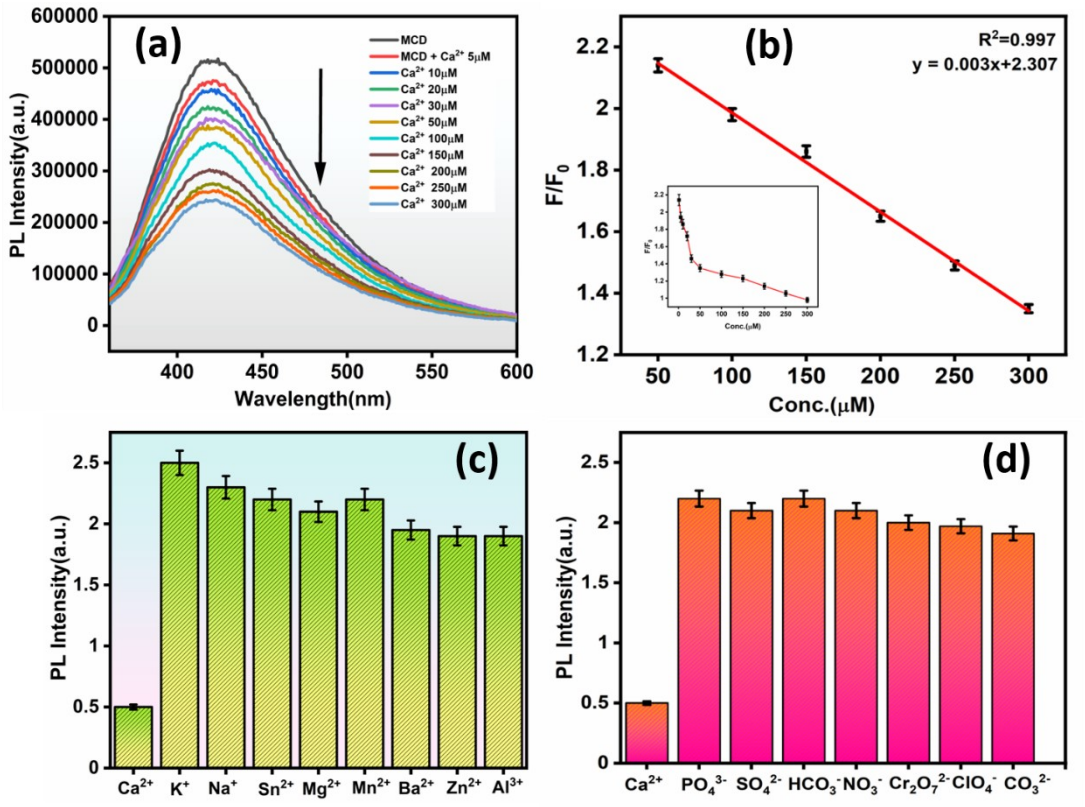

Figure S10 (a)FL detection of Ca^{2+} in aqueous solution (b) linear fitting of detection range (c) selectivity study for cation in aqueous phase (d) selectivity study for anion in aqueous phase

3.5 Fluorescence quenching mechanism

As stated earlier, we believe that the FL quenching of MCDs is a dynamic quenching process. As mention in scheme S2, the EDTA present on surface of the MCDs grabs onto Ca^{2+} ions, eventually leading to the aggregation of MCDs. To evaluate this study, we investigated additional characteristics of the MCDs such as FL lifetime and zeta potential study. Figure S11a displays the FL lifetimes of the MCDs showings 2.09 ns without Ca^{2+} ions and 1.95 ns when Ca^{2+} ions are present. The gap between the two values is very less, falling short of an order of magnitude. It is evident that a dynamic FL quenching mechanism is involved, with the photoluminescence quenching of MCDs in the presence of Ca^{2+} ions likely resulting from a nonradiative energy or electron transfer process.[7] The DLS indicates that the hydrodynamic diameter of CDs significantly rises from 4.5nm to 50nm following the introduction of Ca^{2+} ions (Figure S11b). Analyzing the surface charge of the prepared MCDs before and after adding Ca^{2+} ions through zeta potential analysis will clarify the formation of complexes on the MCDs' surface. The zeta potential of the prepared MCDs were examined to be −4 mV, indicating that

surface is completely functionalized with -Ve charged groups including -COOH group (figure S11c). After the mixing of Ca^{2+} ions, the surface charge of MCD is 2.23 mV, which is due to the formation of a $[Ca\text{-}EDTA]^{2-}$ hexa coordinated octahedral complex on the surface of the MCDs. The findings further validate that the detection of Ca^{2+} ions involve a non-radiative process of electron or energy transfer.

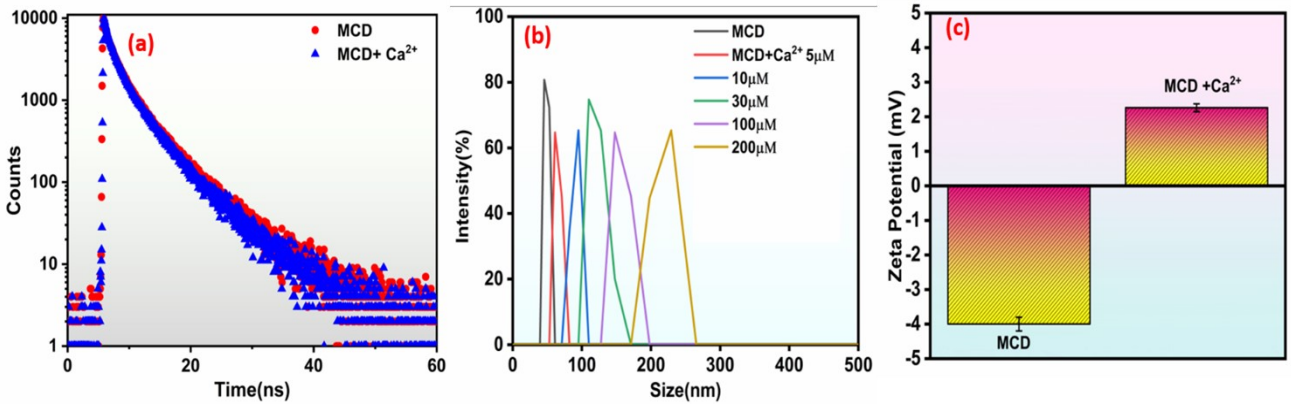

Figure S11 (a)FL life time study of MCD and MCD + Ca^{2+} (b) DLS size MCD and MCD +Ca^{2+} (c)Zeta potential study of MCD and MCD + Ca^{2+}

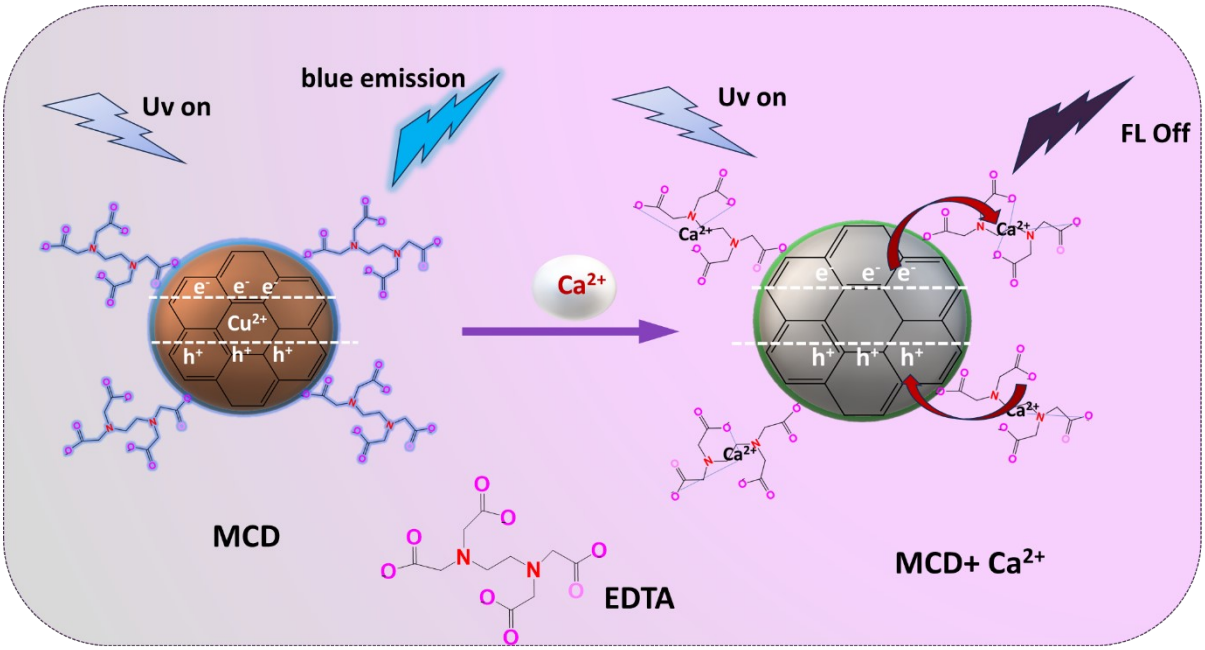

3.6 Repeatability and stability study of MCD@PAGH for Ca^{2+} detection

The reproducibility of the system was investigated by using the relative standard deviation (RSD) of several measurements. To evaluate the repeatability, a series of three MCD@PAGH 2 patch was prepared and calcium detection were carried out on the same day. The calculated RSD% value was

0.40% indicating good repeatability of assay using the MCD@PAGH 2 probe. In addition, the stability of the proposed measurement was investigated over seven days using for a particular concentration of calcium (100µM) solution. The calculated RSD% value was 1.35%, which stability of the proposed sensing protocol. The stability studies of the MCD@PAGH have been mentioned below (fig. S12a, b).

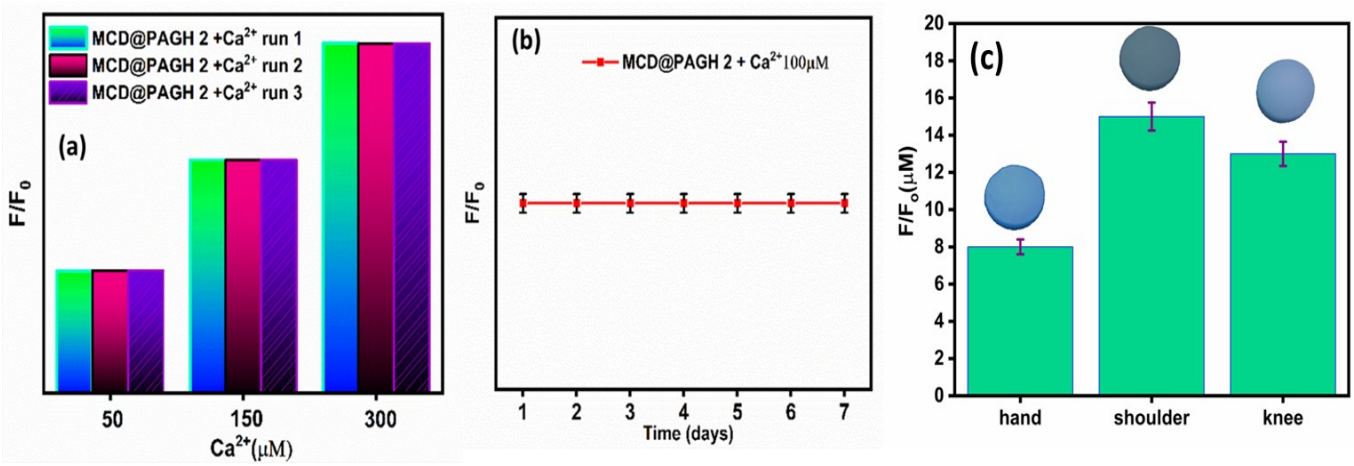

Figure S12 (a) Repeatability study of MCD@PAGH (b) Stability of MCD@PAGH(C) Ca^{2+} ion detection in sweat release from hand, shoulder, knee

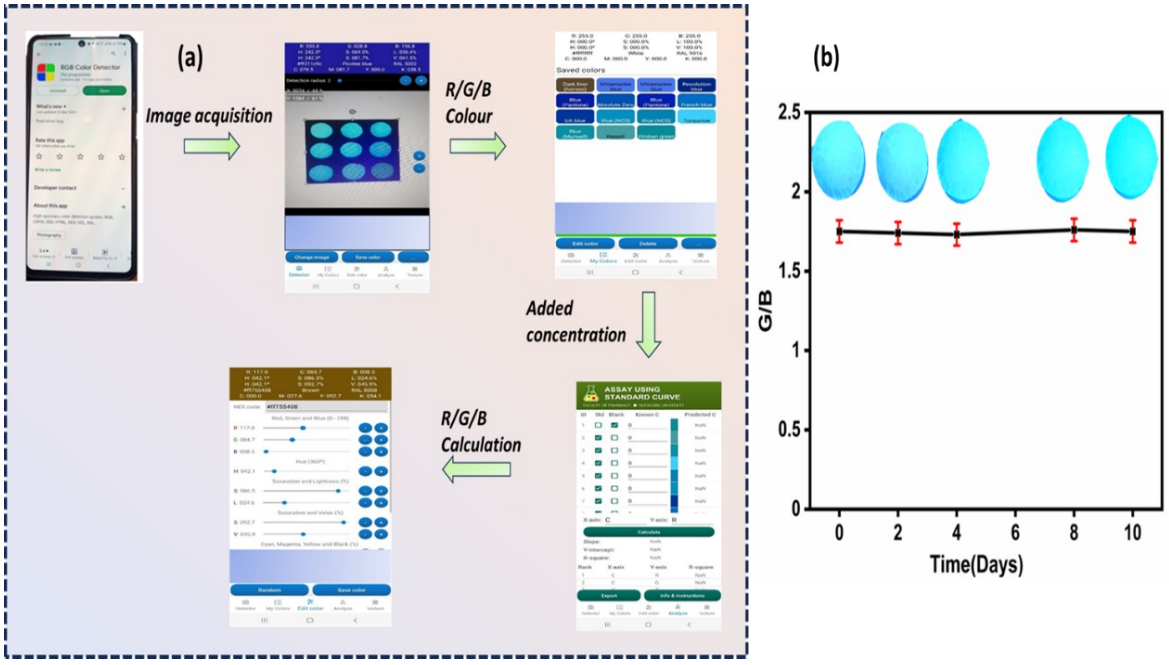

Figure S13(a) RGB-app based detection (b)stability of the MCD@PAGH

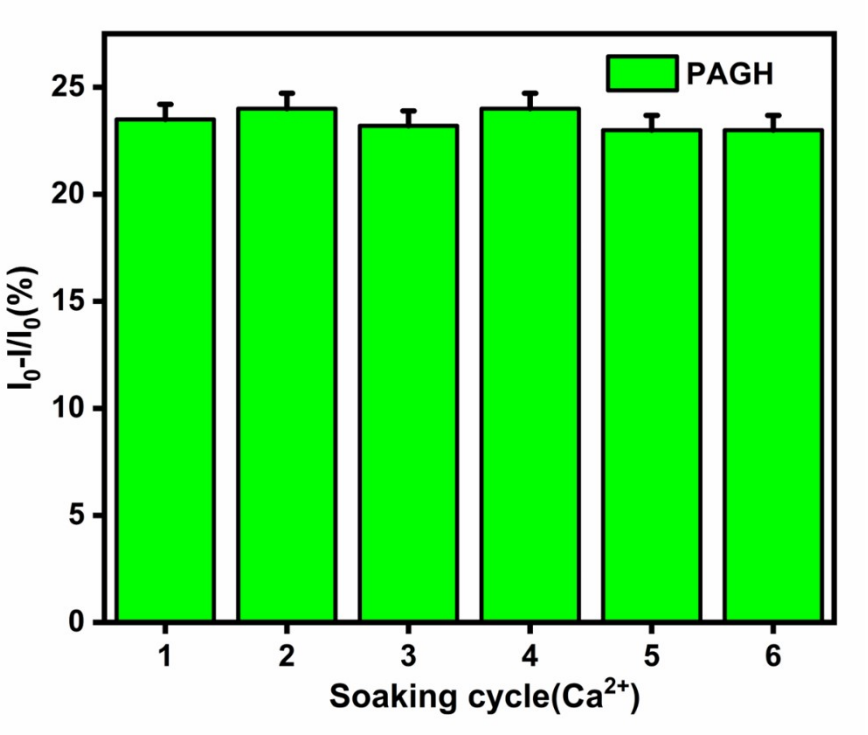

Figure S14 Soaking of Ca^{2+} in PAGH

Table S1. Conditions adopted for MCD@PAGH optimization reaction

Sample No	PVA(g)	Agar(g)	MCD (mg/ml)
PAG	6	1.5	0
MCD@PAG 0.5	6	1.5	0.5
MCD@PAG 2	6	1.5	2
MCD@PAG 4	6	1.5	4

Table S2 Porosity of hydrogel

Hydrogel Name	Pore size (μm)
PAGH	25–35
MCD@PAGH 0.5	18–28
MCD@PAGH 2	15-22
MCD@PAGH 4	15–18

Table S3 A comparison of the mechanical properties and multifunctionality performance of our hydrogel with similar work

Material	Mechanical Properties			Multifunctionality				Reference
	Strength (KPa)	Strain (%)	Toughness (MJ/m^3)	Self-healing	Adhesion	Antibacterial	Biocompatibility	
Agar/Borax/Mxene CH	129	105.1	0.14	√	×	-	-	8
KGM/XG/SA	100	110	0.11	×	-	-	-	9
PVA/SA/chitosan/Mxene	100	263	-	-	-	-	√	10
PVA/borax/starch/TP	70	814	-	-	√	√	-	11
PVA/P(AM-co-SBMA)	370	700	1.3	-	√	√	√	12
gelatin	136	65	0.09	-	√	√	√	13
PAA/ACC/Mxene	-	450	-	-	-	-	√	14
MCD@PAGH	149	164	3.79	√	√	√	√	This work

Table S4 A comparison of the Conductivity, Fluorescence and electrochemical and performance with similar work

Material	Patch based fluorescence sensing of sweat (LOD)	Patch based Electrochemical sensing of sweat (sensing range and LOD)	Reference
PVA/AuNPs@PDA hydrogel	-	0.9 µM	15
CoOOH-modified RENPs	2.037 mM	-	16
CNCs@BSA-GOx/PVA	-	8.2 µM	17
TA-Ag-CNT-PANI	-	3.3 µM	18
PVA/P(AM-co-SBMA) hydrogels	-	-	19
MCD@PAGH	47.51 µM	1mM-1nM	This work

Reference

1. L.Behera, L. Mishra, M. Mishra and S. Mohapatra, Journal of Materials Chemistry B, **2024** 12,5181-5193.
2. X. Xu, and B. Yan. Journal of Materials Chemistry C. **2018**,6, 1863-1869.
3. Y. Zheng, Y. Wang, T. Nakajima, and J. Ping Gong. ACS Macro Letters,**2024**,13 130-137.
4. A. Mohanty, B. C. Pattnayak, L. Behera, A. Singh, S. K. Bhutia, and S. Mohapatra, ACS Applied Bio Materials, **2023**,6, 4314-4325.
5. B. Barik, L. Behera, A. K. Sahu, and S. Mohapatra. Materials Chemistry and Physics, **2023**,307 128188.
6. A.M.N. Alsaif, E. A. Atta, E. Abdeltwab, and M. M. Abdel-Hamid. Macromolecular Research, **2024**,32 35-44.
7. L.Behera, D. Pati, B.B.Sahu, and S. Mohapatra. Colloids and Surfaces A: Physicochemical and Engineering Aspects, **2022**,653, 130002.
8. Z. Nie, K. Peng, L. Lin, J. Yang, Z. Cheng, Q. Gan, Y. Chen, and C. Feng, Chem. Eng. J**. 2023**, 454, 139843.
9. S. Jiang, L. Shang, H. Liang, B. Li, and J. Li, Food Hydrocolloi. **2022**, 127, 107499.
10. T. Wang, J. Wang, Z.Li, M. Yue, X. Qing, P. Zhang, X. Liao, Z. Fan, and S.J. Yang, Appl. Polym. Sci. **2022**, 139, 51627.
11. T. Ke, L. Zhao, X. Fan, and H. Gu. J. Mater. Sci. Technol. **2023**, 135, 199-212
12. Z.Zhou, Z. He, S. Yin, X. Xie, and W. Yuan, Compos. Part B-Eng. **2021**, 220, 108984.
13. Y. Zhang, Q. Wang, Z. Wang, D. Zhang, J. Gu, K. Ye, D. Su, Y. Zhang, J. Chen, and M. Barboiu. ChemPlusChem. **2021**, 86 , 1524-1529.
14. X. B. Li, L. Z. He, Y. F. Li, M. Y. Chao, M. K. Li, P. B. Wan, and L. Q. Zhang, ACS Nano **2021**, 15, 7765.
15. Z.Hou, T. Gao, X. Liu, W. Guo, L. Bai, W. Wang, L. Yang, H. Yang, and D. Wei. International Journal of Biological Macromolecules, **2023**,252, 126473.
16. M.Wang, B. Lin, Y. Chen, H. Liu, Z. Ju, and R. Lv. ACS Biomaterials Science & Engineering, **2024**,10, 1128-1138.
17. J.Liu, L. Pan, W. Wang, L. Bai, H. Chen, L. Yang, K. Yin, H.Yang, and D. Wei Industrial Crops and Products, **2024**,216, 118728.

18. Z.Xu, X. Qiao, R. Tao, Y. Li, S. Zhao, Y. Cai, and X. Luo. Biosensors and Bioelectronics,**2023**,234 115360.

19. Z.Zhou, Z.He, S. Yin, X. Xie, and W. Yuan. Composites Part B: Engineering, **2021**,220 108984.